Applied Chemical Engineering (2026) Volume 9 Issue 2 ISSN: 2578-2010 (O)
doi: 10.59429/ace.v9i2.5934

RESEARCH ARTICLE

DFT Study of Janus SbBrSe Monolayer for Optoelectronic Applications

Ghufran Sattar Khazal[1], Shurooq Sabah Abed Al- Abbas[2*]

[12] *Department of Physics, College of Education for Pure Sciences, University of Babylon, Hilla, Iraq*

***Corresponding author:** Shurooq Sabah Abed Al- Abbas, Pure.Shurooq.sabah@uobabylon.edu.iq

ABSTRACT

Two-dimensional prominent Janus materials have drawn massive interest to enable optoelectronic applications, owing to broken mirror symmetry and adjustable electronic characteristics. In this work, we systematically explore the structural, electronic, and optical properties of the Janus SbBrSe monolayer based on first-principles density functional theory (DFT). Calculated results suggest that the SbBrSe monolayer can be classified as a semiconductor with an effective direct band gap of 1.190 eV located at the Γ point and exhibits a large valley energy difference of ΔE =0.81 eV between the global minimum and secondary valley in conduction bands at Γ and M points, respectively. The material exhibits excellent ultraviolet (UV) light absorption, with a maximum absorption coefficient of 12.2×10^4 cm^{-1} and characteristic peaks at 5.2 eV and 9.8 eV. Interestingly, the negative values of the real dielectric function indicate that the monolayer shows a metallic behavior in the energy range of 5.1-6.5 eV. The SbBrSe monolayer possesses remarkable properties, including a direct bandgap and high absorption in the UV region, rendering it a promising candidate for optoelectronic applications, particularly UV photodetectors.

Keywords: SbBrSe monolayer, semiconductor, UV photodetectors, optoelectronic applications

ARTICLE INFO

Received: 09 March 2026
Accepted: 12 May 2026
Available online: 18 June 2026

1. Introduction

Since graphene was first isolated in 2004 [1], two-dimensional (2D) materials have attracted significant attention and are the subject of extensive research due to their remarkable physical, magnetic, optical, and electronic properties. These properties enable applications in optoelectronics [2], transistors [3], catalytic processes [4], gas sensing technologies [5], photodetectors [6], and electric power storage devices [7]. These materials offer superior flexibility and transparency compared to conventional materials. Given these unique traits, they are strong candidates for future fully transparent electronic and optoelectronic systems. These materials also possess a very high specific surface area due to their atomic thickness, making them beneficial for technologies that require high surface area because of their high surface-to-volume ratio [8,9]. Typically, 2D materials are fabricated by exfoliation from bulk multilayer crystals [10,11]. The TMD monolayers [12 - 14], the IIIA-group metal monochalcogenides [15, 16], and group-VA elements (e.g., phosphorene) [17, 18] are currently the most extensively studied 2D materials after graphene.

Recent advances in exfoliation techniques for 2D materials have led to new paradigms in nanoelectronics. Graphene is challenging to

use in optoelectronic devices since it lacks a bandgap. On the other hand, layered metal chalcogenides represent an excellent strategic choice since they have tunable band gaps (from 0 to > 2.5 eV) and their electrical properties can be modified by compositional changes or mechanical strain [19].

However, monochalcogenide (MX) compounds have certain limitations. For example, they exhibit poor visible light absorption and possess an indirect band gap. Consequently, they are less effective as integrated charge separation systems, making it more difficult to employ them in practical devices like solar panels and optoelectronic devices. Thus, new materials are needed to overcome these issues. In response, a lot of individuals have suggested "Janus crystals," which are asymmetric monolayers of 2D materials. When 2D nanomaterials are exposed to external stimuli, such as chemical changes, external electric fields, mechanical strain, doping, or functionalization with other molecules or materials [20], their electrical characteristics can be significantly altered.

Motivated by the superior properties of Janus architectures and the need for high-efficiency optoelectronic materials, we propose a novel design idea by strategically combining specific advantageous elements. Selenium (Se), a Group VI element, is a well-known chalcogenide semiconductor with a direct bandgap at room temperature [21,22], widely utilized in xerography, highly sensitive imaging, and robust optoelectronic films [23,24]. Bromine (Br) is a highly reactive halogen renowned for its exceptional light-sensitive compounds, such as those used in photographic films [25]. Antimony (Sb) is a stable semi-metal chalcophile element widely used in durable, heat-stable, and flame-retardant industrial applications [26].

In this study, we use first-principles (DFT) simulations to thoroughly examine the physical properties of the two-dimensional SbBrSe monolayer. This work focuses on the material's unique crystal structure, characterized by a buckled arrangement and broken mirror symmetry. We are especially interested in its optical response, band gap, and electronic structure to assess its suitability for future optoelectronic systems.

2. Computational method

Theoretical study was done using DFT-based CASTEP code [27] to investigate the electronic, structural and optical properties of the SbBrSe monolayer. The energy of the exchange-correlation was determined by the PBE functionals combined with OTFG ultrasoft pseudopotentials [28], where the ion-electron interaction was taken into consideration. The relativistic correction was introduced by the Koelling-Harmon approximation. The Monkhorst-Pack mesh of 6×6×2 was adopted for Brillouin zone sampling, which facilitated geometry optimization, and DOS, band structure, and optical responses were predicted. 440 eV cut-off energy of plane wave was considered. Structural relaxation of the SbBrSe monolayer was considered complete when the total energy and interatomic forces converged to 10^{-6} eV and 0.01 eV/Å, respectively. A vacuum slab of approximately 20 Å was introduced to avoid interactions between neighboring layers arising from periodic boundary conditions. To study light-matter interactions, we employed density functional perturbation theory (DFPT). This approach provides various optical parameters including absorption coefficient $\alpha(\omega)$, refractive index $n(\omega)$, reflectivity $R(\omega)$, optical conductivity $\sigma(\omega)$, dielectric function $\varepsilon(\omega)$ and energy loss function $L(\omega)$, where ω denotes the photon frequency. Dielectric function plays a key role in describing a material's response to an external electromagnetic field, as it reveals radiation effects on the medium and the propagation behavior of electromagnetic waves. As presented in [29], the generalized dielectric function can be written as the total of its real and imaginary constituents.

$$\varepsilon(\omega)=\varepsilon_1(\omega)+ i\varepsilon_2(\omega) \quad (1)$$

It is well known that there are connections between the real part $\varepsilon_1(\omega)$ and the imaginary part $\varepsilon_2(\omega)$ [28]. We may determine the real part by using the Kramers-Kronig transformation:

$$\varepsilon_1(\omega)=1+\frac{2}{\pi}P\int_0^{\infty}\frac{\omega'\varepsilon_2(\omega')}{\omega'^2-\omega^2}d\omega'$$

（2）

The integral's principal value is P. The imaginary part of the dielectric function describes the transitions that electrons make between bands. It is given by:

$$\varepsilon_2(\omega)=\frac{2e^2\pi}{\Omega\varepsilon_\circ}\left|<\psi_k^c\left|\hat{u}\times r\right|\psi_k^v>\right|^2\delta(E_k^c-E_k^v-\hbar\omega) \quad (3)$$

Here, e is the electron charge, Ω is the unit cell volume, ε_0 is the vacuum permittivity, and $\hat{u}$ is the polarization vector of the incident radiation. The indices c and v denote the conduction and valence band states, respectively, while ψ_k^c&ψ_k^v represent their corresponding wavefunctions. The integration is performed over the first Brillouin zone.

Furthermore, the complex refractive index is strongly correlated with the dielectric function [29]:

$$\tilde{n}(\omega)= n(\omega)+ik(\omega) \quad (4)$$

Where $n(\omega)$ is the real refractive index and $k(\omega)$ is the extinction coefficient. These parameters are directly obtained from the components of the dielectric function:

$$n(\omega)=\frac{1}{\sqrt{2}}\left[\sqrt{\varepsilon_1^2(\omega)+\varepsilon_2^2(\omega)}+\varepsilon_1(\omega)\right]^{\frac{1}{2}}$$

（5）

$$k(\omega)=\frac{1}{\sqrt{2}}\left[\sqrt{\varepsilon_1^2(\omega)+\varepsilon_2^2(\omega)}-\varepsilon_1(\omega)\right]^{\frac{1}{2}}$$

（6）

The absorption coefficient $\alpha(\omega)$ and the optical conductivity $\sigma(\omega)$ are calculated using the following relations [28]:

$$\alpha(\omega)=\frac{\sqrt{2}\omega}{c}\left[\sqrt{\varepsilon_1^2(\omega)+\varepsilon_2^2(\omega)}-\varepsilon_1(\omega)\right]^{\frac{1}{2}} \quad (7)$$

$$\sigma(\omega)=\frac{\omega}{4\pi}\varepsilon_2(\omega) \quad (8)$$

Where c stands for the speed of light in a vacuum. Finally, the normal-incidence reflectivity R(ω) and the energy loss function L(ω), which describes the energy lost by fast-moving electrons traversing the material, are evaluated as follows [29]:

$$R(\omega)=\frac{[n(\omega)-1]^2+k^2(\omega)}{[n(\omega)+1]^2+k^2(\omega)} \quad (9)$$

$$L(\omega)=\frac{\varepsilon_2(\omega)}{\varepsilon_1^2(\omega)+\varepsilon_2^2(\omega)} \quad (10)$$

3. Discussion and Conclusion

3.1. Electronic Properties

We were able to figure out the structural and geometric parameters of the SbBrSe monolayer after thoroughly relaxing the structure. Figure 1 shows these traits. The geometry optimization reveal exactly how long and at what angles the bonds that make up the crystal structure are. The distance between antimony and bromine atoms (d_{Sb-Br}) was 2.959 Å, whereas the distance between antimony and selenium atoms (d_{Sb-Se}) was 3.045 Å. The distance between selenium and bromine atoms (d_{Se-Br}) was likewise found to be 4.209 Å. The calculations showed that the angle between Sb-Se-Sb is 89.290° and the angle between Se-Sb-Se is 80.290°. The bond angles for both Sb-Br-Sb and Br-Sb-Br were also 92.647°. The angle between the Br-Se-Br bonds was 61.118°. These numbers illustrate exactly what the crystal structure looks like and confirm its optimized configuration.

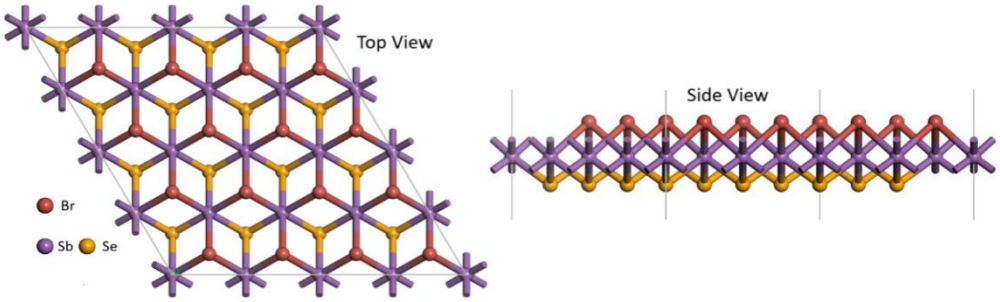

Figure 1. Top and side views of a Janus SbBrSe monolayer's geometric crystal structure.

The electronic properties of the SbBrSe monolayer are illustrated in Figure 2. Figure 2a presents the total density of states (TDOS) and orbital-projected partial density of states (PDOS), while Figure 2b shows the calculated electronic band structure.

As seen in Fig. 2a, the valence band maximum (VBM) is primarily composed of p-orbitals, with minor contributions from s-orbitals. The conduction band minimum (CBM) is also dominated by p-orbitals. The PDOS analysis confirms that p-orbitals of the constituent elements (Sb, Br, and Se) are the main contributors to electronic states near the Fermi level, which is consistent with the semiconducting nature of the material.

Regarding the band structure in Fig. 2b, this material has a direct band gap, as shown by the results. The band gap of the SbBrSe monolayer is 1.190 eV, which makes it behave like a semiconductor. Γ, the point of symmetry, is quite near to both the VBM and the CBM, the valence band maximum and conduction band minimum, respectively. Crucially, the energy difference between the global minimum at (Γ) and the secondary local minimum at the M point is about 0.81 eV. Direct electron transitions usually occur near the (Γ) point because they do not require a change in momentum. Consequently, light may be absorbed far more easily. It should be noted that the calculated band gap from the PBE functional may be slightly underestimated compared to experimental values, which is a common limitation for DFT-based approaches. Nevertheless, the SbBrSe monolayer is well-suited for use in optoelectronics and photocatalysis since its band gap is direct and has been precisely adjusted through its Janus structure.

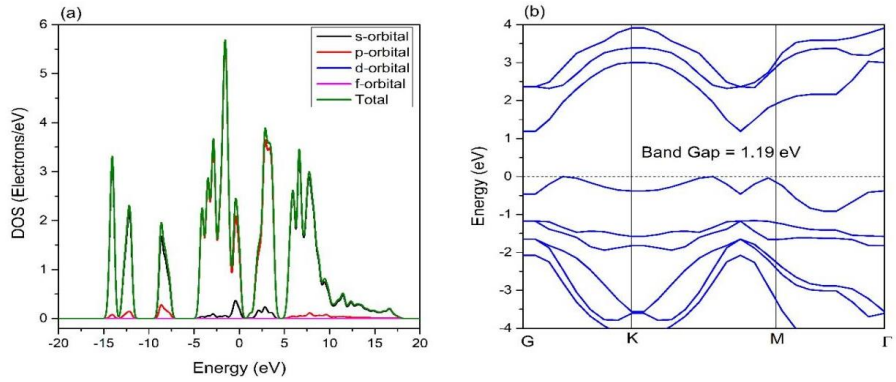

Figure 2. Calculated electronic band structure of the SbBrSe monolayer.

3.2. Optical Properties

Optical properties play a key role when selecting materials for photodetectors and optoelectronic devices. In this work, we examined the optical behavior of the SbBrSe monolayer across a photon energy range of up to 35 eV. The frequency-dependent complex dielectric function reveals several notable optical features. Figure 3 presents the real and imaginary parts of the calculated dielectric function as a function of photon energy.

It is evident from Figure 3 that there are distinct peaks in the dielectric function's real and imaginary components. Near 4.0 eV is the most significant peak in the real part, and around 4.9 eV is the most significant peak in the imaginary part. The large and distinct peak in the imaginary dielectric function indicates a significant electronic transition from the valence band to the conduction band. The low-energy region has the most prominent peaks of the dielectric constant; therefore, it stands to reason that the majority of the photons that reach the surface are reflected there. Approximately the same size as the real peak is the largest peak in the area of the SbBrSe monolayer that is envisioned. Similar to other 2D materials, the highest peak intensity of the SbBrSe monolayer's real part is comparable. We found that for zero photon energy, the static dielectric constant is about 3.0. This value indicates that the electronic polarizability of the monolayer is extremely high. This static dielectric constant should also be present in very tiny materials. Since the dielectric constant is an important factor in determining the amount of charge stored in a capacitor, this static value implies that it could be valuable for constructing capacitors.

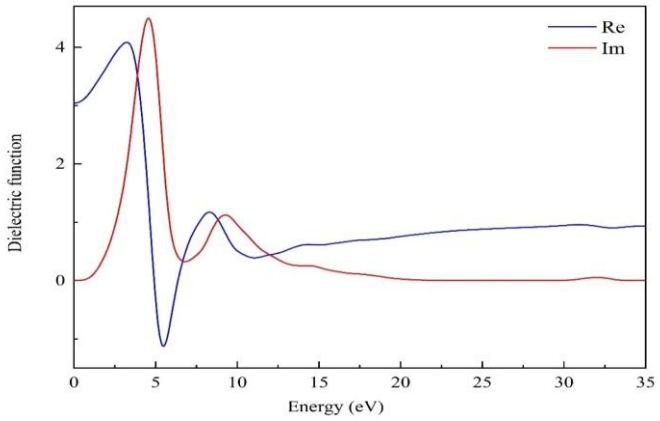

Figure 3. Dielectric Function of SbBrSe monolayer.

Lastly, the data shows that the SbBrSe monolayer behaves like a metal in the energy range of approximately 5.1 eV to 6.5 eV. This region of the electromagnetic spectrum exhibits negative values for the real dielectric function, which explains the phenomenon. The material absorbs a large amount of light with

energies between 3 and 13 eV, as shown in Figure 4 of the optical absorption spectra. The most important factor is that the SbBrSe monolayer starts to absorb visible light at around 2.0 eV. Two peaks can be observed from the graph at energies of 5.2 eV and 9.8 eV, respectively. The above layer can effectively absorb a number of photons in the UV range. It can be inferred from the above peaks that the SbBrSe monolayer is appropriate for the operation of UV photoelectric and optoelectronic devices. The value of the absorption coefficient for the SbBrSe monolayer is approximately 12.2×10^4 cm^{-1}.

The optical conductivity of the SbBrSe monolayer changes with varying photon energy, as seen in Figure 5. Spectroscopic analysis confirms that the material is a semiconductor. The optical conductivity begins at the band gap energy, which is around 2.0 eV. The real part shows a strong optical peak at 4.75 eV. The highest interaction between photons and electrons occurs in the ultraviolet (UV) spectrum, resulting in its highest optical conductivity. These features make the SbBrSe monolayer a great material for UV photodetectors.

The energy loss function shifts in relation to the photon energy, as illustrated in Figure 6. The SbBrSe monolayer has a robust peak at 6.4 eV. The material's plasma frequency differentiates its dielectric and metallic characteristics. The bulk of the energy is lost at that point. The material displays dielectric characteristics at energies lower than the plasma frequency. Its behavior resembles that of a metal once it passes this point. The loss function peak for this monolayer is in the UV region.

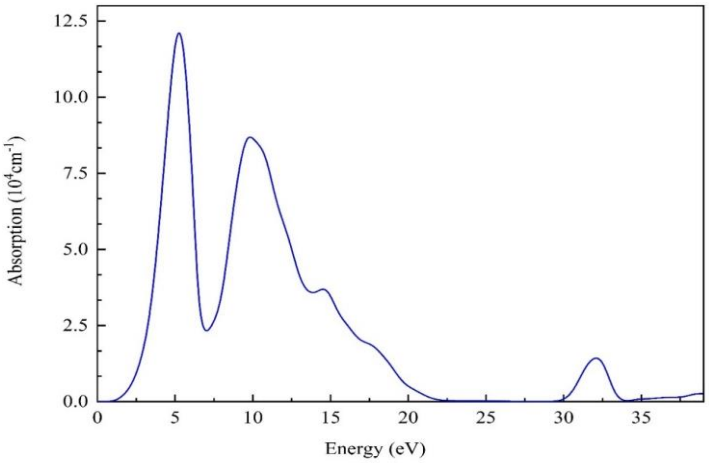

Figure 4. Absorption Coefficient of SbBrSe monolayer.

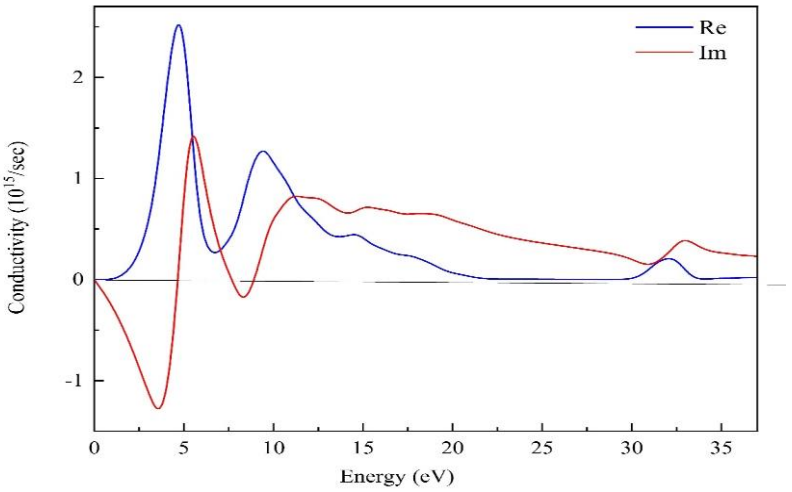

Figure 5. Conductivity of SbBrSe monolayer

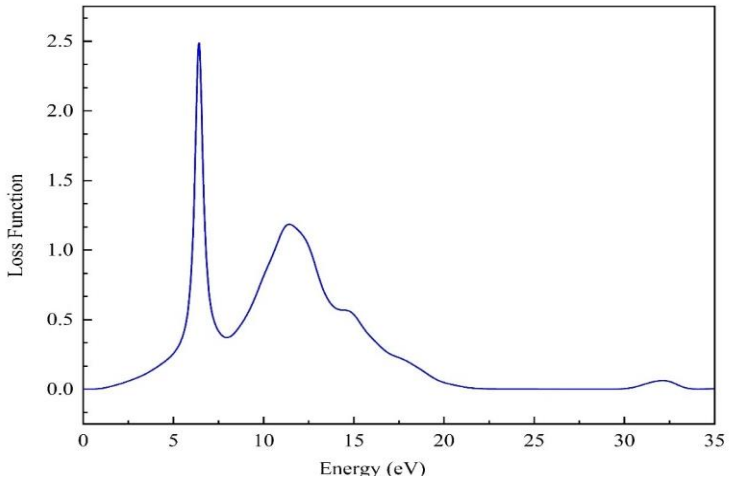

Figure 6. Loss function of SbBrSe monolayer

The relationship between photon energy and the SbBrSe monolayer's refractive index is illustrated in Figure 7. The static refractive index is 1.75 at zero photon energy. The refractive index peaks at 2.10 at a photon energy of 3.6 eV. The refractive index gradually drops after this high, although it stays quite close to one at higher energies. At 5.2 eV, the imaginary part, which represents the extinction coefficient, reaches its maximum value of 1.46. This is confirmed by every other optical parameter. Our research proves that building optoelectronic devices from the SbBrSe monolayer is a promising endeavor.

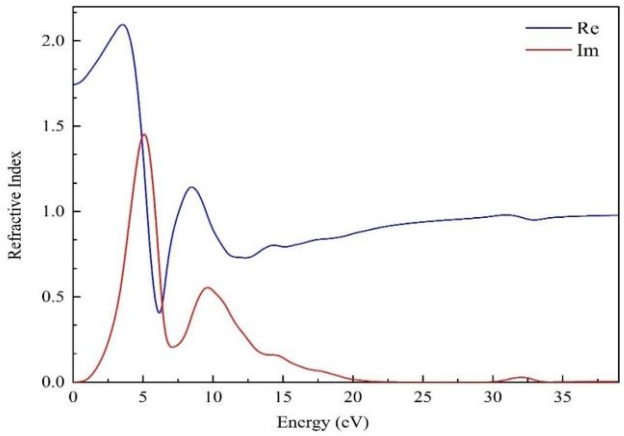

Figure 7. Refractive Index (n) of SbBrSe monolayer.

The optical response of the SbBrSe monolayer can be understood in terms of its electronic band structure and density of states. The absorption peak observed at 5.2 eV corresponds to electronic transitions from the p-orbitals in the valence band (located between -5 eV and the Fermi level) to the p-orbitals in the conduction band (between 0 and 5 eV), as confirmed by the PDOS analysis in Fig. 2a. The prominent peak in the imaginary part of the dielectric function at 4.9 eV originates from direct interband transitions near the Γ point, where both the VBM and CBM are located (Fig. 2b). The onset of optical absorption at approximately 2.0 eV coincides with the direct band gap energy of 1.190 eV, considering the typical underestimation of the PBE functional. The sharp peak in optical conductivity at 4.75 eV results from increased coupling of photons with electrons because of the high concentration of p-orbitals at the Fermi level. The metallic character seen in the 5.1-6.5 eV range, evidenced by negative values of real parts of the dielectric function, is in accordance with no available electronic transitions in that region, according to the DOS. Therefore, the consistency between

the optical data and electronic structure of the material demonstrates that SbBrSe is a suitable choice for UV optoelectronic devices.

4. Conclusion

We studied the optical, electronic, and structural properties of the SbBrSe monolayer using first-principles simulations. Our calculations show that the SbBrSe monolayer acts like a semiconductor with a direct band gap of 1.190 eV at the Γ point, where we find the maximum of the valence band and the minimum of the conduction band. There is a large energy difference of about 0.81 eV between the secondary valley and the global minimum of the conduction band at the M-point. This indirect valley cannot be filled due to this significant energy gap. As a result, direct inter-band transitions are more common. This property improves optical absorption in phonon-free environments. The SbBrSe monolayer shows negative values for the real dielectric function, indicating metallic behavior in the 5.1 – 6.5 eV range of the electromagnetic spectrum. This suggests it may be suitable for capacitor applications. Furthermore, the material's strong absorption of ultraviolet light points to possible use as a photocatalyst or photodetector. We hope these findings will inspire researchers to further explore the development and use of functional optoelectronic devices based on SbBrSe monolayers. These results will also provide useful insights for future experimental and theoretical research.

References

1. K. S. Novoselov, A. K. Geim, S. V. Morozov, D. Jiang, Y. Zhang, S. V. Dubonos, I. V. Grigorieva, and A. A. Firsov, "Electric field effect in atomically thin carbon films," *Science*, vol. 306, pp. 666 – 669, 2004. DOI: 10.1126/science.1102896.
2. M. Shanmugam, T. Bansal, C. A. Durcan, and B. Yu, "Molybdenum disulphide/titanium dioxide nanocomposite-poly 3-hexylthiophene bulk heterojunction solar cell," *Appl. Phys. Lett.*, vol. 100, p. 153901, 2012. DOI: 10.1063/1.3703602.
3. B. Radisavljevic, A. Radenovic, J. Brivio, V. Giacometti, and A. Kis, "Integrated circuits and logic operations based on single-layer MoS2," *ACS Nano*, vol. 5, pp. 9934 – 9938, 2011. DOI: 10.1021/nn203715c.
4. H. R. Jappor and A. S. Jaber, "Electronic properties of CO and CO2 adsorbed silicene/graphene nanoribbons as a promising candidate for a metal-free catalyst and a gas sensor," *Sensor Letters*, vol. 14, pp. 989 – 995, 2016. DOI: 10.1166/sl.2016.3722.
5. H. R. Jappor and S. A. M. Khudair, "Electronic properties of adsorption of CO, CO2, NH3, NO, NO2 and SO2 on nitrogen doped graphene for gas sensor applications," *Sensor Letters*, vol. 15, no. 5, pp. 432 – 439, 2017. DOI: 10.1166/sl.2017.3819.
6. P. Hu, Z. Wen, L. Wang, P. Zheng, and J. Fang, "Highly responsive ultrathin GaS nanosheet photodetectors on rigid and flexible substrates," *Nano Lett.*, vol. 13, pp. 1649 – 1654, 2013. DOI: 10.1021/nl400107k.
7. X. Zhang, Z. Lai, C. Tan, and H. Zhang, "2D materials beyond graphene for high-performance energy storage applications," *Adv. Energy Mater.*, vol. 6, p. 1600671, 2016. DOI: 10.1002/aenm.201600671.
8. Y. Li, Y.-L. Li, B. Sa, and R. Ahuja, "Review of two-dimensional materials for photocatalytic water splitting from a theoretical perspective," *Catal. Sci. Technol.*, vol. 7, pp. 545 – 559, 2017. DOI: 10.1039/C6CY02178F.
9. M. D. Stoller, S. Park, Y. Zhu, J. An, and R. S. Ruoff, "Graphene-based ultracapacitors," *Nano Lett.*, vol. 8, pp. 3498 – 3502, 2008. DOI: 10.1021/nl802558y.
10. C. Huo, Z. Yan, X. Song, and H. Zeng, "2D materials via liquid exfoliation: A review on fabrication and applications," *Science Bulletin*, vol. 60, p. 1994, 2015. DOI: 10.1007/s11434-015-0936-3.
11. L. Yuan, J. Ge, X. Peng, Q. Zhang, Z. Wu, Y. Jian, X. Xiong, H. Yin, and J. Han, "A reliable way of mechanical exfoliation of large scale two dimensional materials with high quality," *AIP Advances*, vol. 6, p. 125201, 2016. DOI: 10.1063/1.4967967.
12. R. Li, Y. Cheng, and W. Huang, "Recent progress of Janus 2D transition metal chalcogenides: From theory to experiments," *Small*, vol. 14, no. 45, p. 1802091, 2018. DOI: 10.1002/smll.201802091
13. M. Chhowalla, Z. Liu, and H. Zhang, "Two-dimensional transition metal dichalcogenide (TMD) nanosheets," *Chem. Soc. Rev.*, vol. 44, pp. 2584 – 2586, 2015. DOI: 10.1039/c5cs90037a.
14. K. Kalantar-zadeh and J. Z. Ou, "Two-dimensional transition metal dichalcogenides in bio systems," *Adv. Funct. Mater.*, vol. 25, pp. 5086 – 5099, 2015. DOI: 10.1002/adfm.201501861.

15. A.Castellanos-Gomez, “Why all the fuss about 2D group-III monochalcogenides? *Nature Photonics*, vol. 10, pp. 202 – 204, 2016. DOI: 10.1038/nphoton.2016.53
16. H. R. Jappor and M. A. Habeeb, "Optical properties of two-dimensional GaS and GaSe monolayers," *Physica E: Low-dimensional Systems and Nanostructures*, vol. 101, pp. 251 – 255, 2018. DOI: 10.1016/j.physe.2018.04.019.
17. V. Eswaraiah, Q. S. Zeng, Y. Long, and Z. Liu, "Black phosphorus nanosheets: Synthesis, characterization and applications," *Small*, vol. 12, pp. 3480 – 3502, 2016. DOI: 10.1002/smll.201600032.
18. J. Pei, X. Gai, J. Yang, X. Wang, Z. Yu, D.-Y. Choi, B. Luther-Davies, and Y. Lu, "Producing air-stable monolayers of phosphorene and their defect engineering," *Nat. Commun.*, vol. 7, p. 10450, 2016. DOI: 10.1038/ncomms10450.
19. G. Fiori, F. Bonaccorso, G. Iannaccone, T. Palacios, D. Neumaier, A. Seabaugh, S. K. Banerjee, and L. Colombo, "Electronics based on two-dimensional materials," *Nature Nanotechnology*, vol. 9, no. 10, pp. 768 – 779, 2014. DOI: 10.1038/nnano.2014.207.
20. A. E. Sudheer, A. Kumar, G. Tejaswini, M. Vallinayagam, M. Posselt, M. Zschornak, C. Kamal, and D. Murali, “A first principles study on the stability and electronic and optical properties of 2D SbXY (X = Se/Te and Y = I/Br) Janus layers,” *Phys. Chem. Chem. Phys.*, vol. 26, pp. 29371 – 29383, 2024, doi: 10.1039/D4CP04077E.
21. Y. Wang, C. Li, W. Chen, Y. Li, and L. Meng, “Elemental 2D materials: Selenene and tellurene,” *J. Semicond.*, vol. 41, no. 8, p. 081001, 2020, doi: 10.1088/1674-4926/41/8/081001.
22. M. Barhoumi, I. Said, N. Sfina, N. K. Al-Saleem, and T. Ghrib, “A DFT study of the electronic and optical properties of four 2D thin films,” *Mater. Chem. Phys.*, vol. 286, p. 126158, 2022, doi: 10.1016/j.matchemphys.2022.126158.
23. A. Bafekry, M. Faraji, M. M.Fadlallah, D. M. Hoat, H. R. Jappor, I. A. Sarsari, M. Ghergherehchi, and S. A. H. Feghhi, “Electronic, optical and thermoelectric properties of a novel two-dimensional SbXY (X = Se, Te; Y = Br, I) family: ab initio perspective,” *Phys. Chem. Chem. Phys.*, vol. 23, pp. 25866 – 25876, 2021, doi: 10.1039/D1CP03706D.
24. M. Shen, Y. Yu, C. Liu, L. Ju, M. Chen, and H. Yin, “Promising optoelectronic properties and potential infrared photodetection applications of two-dimensional monolayer $PdTeI_2$,” *Results Phys.*, vol. 53, p. 106935, 2023, doi: 10.1016/j.rinp.2023.106935.
25. T. H. James, “Selective latent image distribution in silver halides,” J. Imaging Sci., vol. 28, no. 5, pp. 204 – 210, 1984, doi: 10.1080/00223638.1984.11738285.
26. N. Niasadegh, M. Naseri, and S. Rezaee, “Visible light response in 2D QBi (Q = Si, Ge and Sn) monolayer semiconductors: A DFT based study,” *Mater. Today Commun.*, vol. 35, p. 105886, 2023, doi: 10.1016/j.mtcomm.2023.105886.
27. S. J. Clark, M. D. Segall, C. J. Pickard, P. J. Hasnip, M. I. J. Probert, K. Refson, and M. C. Payne, "First principles methods using CASTEP," Z. Kristallogr., vol. 220, pp. 567 – 570, 2005. DOI: 10.1524/zkri.220.5.567.65075.
28. J. P. Perdew, K. Burke, and M. Ernzerhof, "Generalized gradient approximation made simple," Phys. Rev. Lett., vol. 77, pp. 3865 – 3868, 1996. DOI: 10.1103/PhysRevLett.77.3865.
29. S. S. Abed Al-Abbas, M. K. Muhsin, and H. R. Jappor, "Tunable optical and electronic properties of gallium telluride monolayer for photovoltaic absorbers and ultraviolet detectors," Chemical Physics Letters, vol. 713, pp. 46-51, Dec. 2018. DOI: 10.1016/j.cplett.2018.10.020.